Journal of Alloys and Compounds 623 (2015) 324–327

Contents lists available at ScienceDirect

Journal of Alloys and Compounds

journal homepage: www.elsevier.com/locate/jalcom

Electrical properties of fluorine-intercalated layered manganite: $La_{1.4}Sr_{1.6}Mn_2O_7F_2$

Ankam Bhaskar, C.-S. Sheu, Chia-Jyi Liu *

Department of Physics, National Changhua University of Education, Changhua 500, Taiwan

ARTICLE INFO

Article history:
Received 14 August 2014
Received in revised form 8 October 2014
Accepted 20 October 2014
Available online 28 October 2014

Keywords:
Ceramics
Sintering
Exchange and superexchange
X-ray diffraction

ABSTRACT

Fluorinating agent NH_4F is employed to intercalate the bi-layered manganite $La_{1.4}Sr_{1.6}Mn_2O_7$ to form $La_{1.4}Sr_{1.6}Mn_2O_7F_2$ using solid state reaction. The insertion of fluorine results in a contraction of ~0.116 Å in the *a* axis and an expansion of ~3.152 Å in the *c* axis with respect to the parent compound $La_{1.4}Sr_{1.6}Mn_2O_7$. The Mn–O bond lengths are altered due to the electrostatic repulsion between O^{2-} and F^-. Rietveld analysis indicates that a longer bond length of Mn–O(1) and shorter bond lengths of Mn–O(2) and Mn–O(3) has been found in $La_{1.4}Sr_{1.6}Mn_2O_7F_2$ when compared to $La_{1.4}Sr_{1.6}Mn_2O_7$. The electrical resistivity of $La_{1.4}Sr_{1.6}Mn_2O_7F_2$ shows insulating behavior and exhibits remarkably different behavior from $La_{1.4}Sr_{1.6}Mn_2O_7$. For the first time, we report the temperature dependence of electrical resistivity of $La_{1.4}Sr_{1.6}Mn_2O_7F_2$. Magnetic measurements indicate that the magnetic order of local moments is suppressed by fluorine insertion into interstitial sites.

1. Introduction

In recent years, great attention has been paid to the series of Ruddlesden–Popper compounds $(RE, AE)_{n+1}Mn_nO_{3n+1}$ with perovskite-like structure, where RE is a trivalent rare-earth cation and AE a divalent alkaline-earth cation, due to the existence of an extraordinary colossal magnetoresistance (CMR) effect [1,2]. A large magnetoresistance is subsequently discovered in $La_{2-2x}Sr_{1+2x}Mn_2O_7$ with $x = 0.3$ and 0.4 [3–8]. Fluorine insertion reaction has been shown by modifying the structure of materials [9]. Recently, the insertion of fluorine into mixed copper oxides is adopted to control the carrier density and, hence, induces superconductivity [10,11]. This idea has been implemented to other oxide systems such as $Sr_2TiO_3F_2$ [12], $Ba_2ZrO_3F_2{\cdot}0.5H_2O$ [13], $Sr_3Mn_2O_6F_y$ with $y = 1$, 2 and 3 [14], $Sr_2TiO_3F_2$ and $Ca_2CuO_2F_2$ [15], $Ln_{1.2}Sr_{1.8}Mn_2O_7F_2$ (Ln = Pr, Nd, Sm, Eu, and Gd) [16]. The fluorine intercalation layered manganites $LaSrMnO_4F$, $La_{1.2}Sr_{1.8}Mn_2O_7F$ and $La_{1.2}Sr_{1.8}Mn_2O_7F_2$ can be prepared from $LaSrMnO_4$ ($n = 1$) and $La_{1.2}Sr_{1.8}Mn_2O_7$ [9,16–19]. The fluorination proceeds in an oxidative manner with fluorine being inserted into interstitial sites between the (La/Sr)O rocksalt layers. This leads to a significant expansion in the *c*-axis as the separation between perovskite blocks is increased. The overall structure of the perovskite blocks is preserved, but is noticeably distorted with the apical Mn–O bond directed towards the rocksalt layers being significantly shorter than that in the center of the perovskite blocks [17]. A variety of fluorinating agents such as F_2 gas, NH_4F, CuF_2 or poly(vinylidene fluoride) (PVDF) can be used to prepare $LaSrMnO_4F$ and $Ln_{1.2}Sr_{1.8}Mn_2O_7F_2$ [16–18]. To the best of our knowledge, there is neither previous report on the electrical properties of the $LaSrMnO_4F$, $La_{1.2}Sr_{1.8}Mn_2O_7F$, $Ln_{1.2}Sr_{1.8}Mn_2O_7F_2$ [16–19] nor the synthesis of $La_{1.4}Sr_{1.6}Mn_2O_7F_2$. Therefore, it would be interesting to investigate the electrical properties of $La_{1.4}Sr_{1.6}Mn_2O_7F_2$.

2. Experimental details

$La_{1.4}Sr_{1.6}Mn_2O_7$ powder was synthesized by quantitatively mixing high-purity powders of La_2O_3, $SrCO_3$ and Mn_2O_3. The mixed and ground powders were then calcined at 1490 °C in oxygen for 36 h with intermediate grindings. The resulting powders were sintered at 1500 °C in air for 24 h, followed by annealing at 800 °C under nitrogen atmosphere. $La_{1.4}Sr_{1.6}Mn_2O_7$ was ground with fluorinating agent (NH_4F) (1:3 molar ratio). The resulting mixing powders were made into a parallelepiped and then sintered at 350 °C for 24 h in the flowing N_2 gas [16–18]. The resulting parallelepiped sample was then ground into powders and then mixed with additional NH_4F (1:1 molar ratio). The resulting mixture was ground and pressed into a parallelepiped, which is then sintered at 350 °C for another 24 h in the flowing N_2 gas [16–18]. In order to deprive some oxygen extent, the parallelepiped was loaded into a Pyrex ampoule along with titanium metal, which is used as a getter for trace amounts of oxygen in the ampoule. The ampoule was evacuated using a diffusion pump to reach a vacuum up to 10^{-5} to 10^{-6} torr and then sealed. After that the ampoule was placed into a box furnace for sintering at various temperatures. The phase purity of resulting powders was examined by a Shimadzu XRD-6000 powder X-ray diffractometer equipped with Cu Kα radiation. The electrical resistance measurements were carried out using the constant voltage method with a Keithley 6512 electrometer. A commercial superconducting quantum interference device magnetometer (Quantum Design) was used to characterize the magnetic properties of the samples.

---

* Corresponding author. Tel.: +886 4 723 2105x3337; fax: +886 4 728 0698.
E-mail address: liucj@cc.ncue.edu.tw (C.-J. Liu).

http://dx.doi.org/10.1016/j.jallcom.2014.10.099
0925-8388/

3. Results and discussion

Figs. 1a and b show the X-ray diffraction (XRD) patterns of $La_{1.4}Sr_{1.6}Mn_2O_7$ and $La_{1.4}Sr_{1.6}Mn_2O_7F_2$ at various post-annealing temperatures. All the diffraction peaks of $La_{1.4}Sr_{1.6}Mn_2O_7$ can be indexed based on the tetragonal structure with the space group *I4/mmm* [7], and no secondary phase is detected. The XRD pattern of $La_{1.4}Sr_{1.6}Mn_2O_7$ is consistent with earlier reports [7,20,21]. The XRD patterns of $La_{1.2}Sr_{1.8}Mn_2O_7F_2$ are matched with earlier reports [7,16,17]. However, a tiny amount of impurity phase (La, Sr)MnO_3 is detected for $La_{1.2}Sr_{1.8}Mn_2O_7F_2$. Sivakumar and Wiley [16] and Greaves et al. [17] have also detected a little amount of impurity phase in $Ln_{1.2}Sr_{1.8}Mn_2O_7F_2$. Fig. 2 shows the schematic structure of $La_{1.4}Sr_{1.6}Mn_2O_7F_2$, where the fluorine is inserted into interstitial sites. Powder diffraction patterns of all the samples are refined using the Rietveld refinement method for structural characterization. All the structural parameters are tabulated in Table 1. Both the lattice constants of *a* and *c* of the parent material are closely matched with earlier reports [22–24]. The *a* axis of $La_{1.4}Sr_{1.6}Mn_2O_7F_2$ decreases by ~0.116 Å, while the *c*-axis increases by ~3.152 Å with respect to the parent material. Similar tendency was observed for $Ln_{1.2}Sr_{1.8}Mn_2O_7F_2$ [16,17]. These results suggest that the fluorine ions are inserted into interstitial sites between the two rock-salt layers, which leads to a significant expansion in the *c* axis. As shown in Fig. 2, the two apical Mn–O bonds, labeled as Mn–O(1) and Mn–O(2) and the four equatorial Mn–O(3) bond lengths are distorted by fluorine ion insertion into interstitial sites. The manganese cations might be shifted away from the center of the MnO_6 octahedron, towards the interstitial site, while the other anions relax in the opposite direction [9,18]. The Mn–O(1) bond length of the parent system is shorter than that of $La_{1.4}Sr_{1.6}Mn_2O_7F_2$; both the bond lengths of Mn–O(2) and Mn–O(3) for the parent compound are longer than Mn–O(2), Mn–O(3) of $La_{1.4}Sr_{1.6}Mn_2O_7F_2$ due to the fluorine ion insertion into interstitial sites. As a result, the difference between the equatorial and the apical Mn–O bond length of $La_{1.4}Sr_{1.6}Mn_2O_7F_2$ decreases as compared to $La_{1.4}Sr_{1.6}Mn_2O_7$, which might arise from the reduction or even the absence of Jahn–Teller ion of Mn^{3+}. The Mn^{3+} with d^4 electron configuration would cause Jahn–Teller distortion such as axial elongation along the *c* axis; the *c*-axis elongation can be seen for the parent compound having longer Mn–O(2) bond length than Mn–O(1). Besides, the Mn–O(2) bond length is shorter than Mn–O(1) bond length for $La_{1.4}Sr_{1.6}Mn_2O_7F_2$ due to the electrostatic repulsion between O(2) and F anions [19]. The refinement statistics (R_P, R_{wp}, R_{exp} and χ^2) are significantly improved by inclusion of fluorine ion. The structural parameters clearly demonstrate the fluorine ion insertion into interstitial sites which in turn is expected to affect the electrical properties.

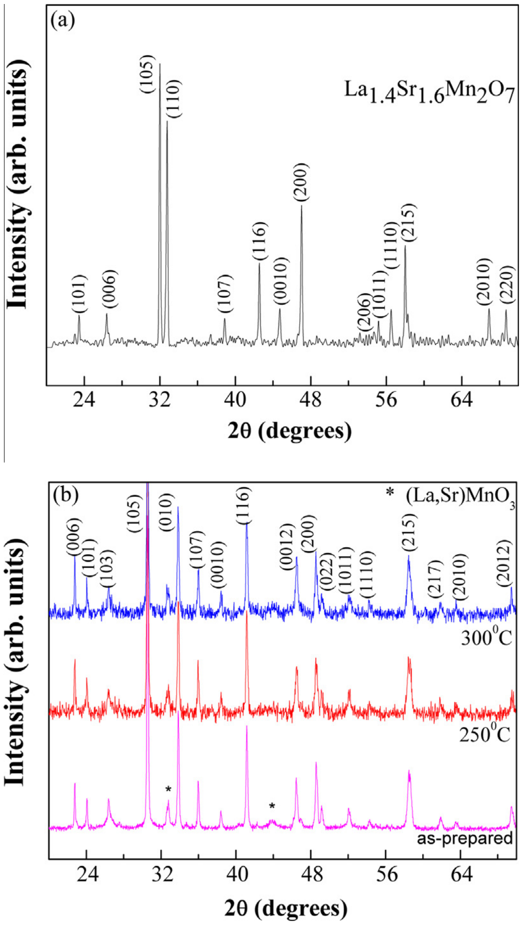

Fig. 1. XRD patterns of $La_{1.4}Sr_{1.6}Mn_2O_7$ (a), and $La_{1.4}Sr_{1.6}Mn_2O_7F_2$ at various post-annealing temperatures (b).

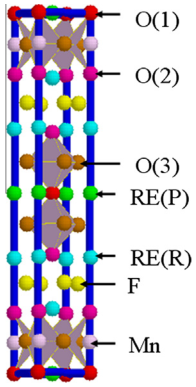

Fig. 2. The crystal structure of $La_{1.4}Sr_{1.6}Mn_2O_7F_2$, P and R refer 12- and 9-coordinate cations, respectively.

Table 1
Cell parameters, Mn–O bond lengths, Rietveld refinement indices (R_P, R_{wp}, R_{exp} and χ^2) at room temperature for all the samples.

Samples	Parent	As-prepared	Ti-250 °C	Ti-300 °C
a (Å)	3.8632(4)	3.7479(7)	3.7493(7)	3.7492(7)
c (Å)	20.2965(4)	23.4488(8)	23.4344(8)	23.4347(8)
Mn–O(1) (Å)	1.9550(4)	2.0077(6)	2.0200(6)	2.0233(6)
Mn–O(2) (Å)	2.0829(1)	1.8218(2)	1.8206(2)	1.8150(2)
Mn–O(3) (Å)	1.9330(7)	1.8756(7)	1.8777(9)	1.8778(1)
R_P (%)	4.21	3.88	3.91	3.87
R_{wp} (%)	5.66	5.15	5.26	5.13
R_{exp} (%)	3.70	3.56	3.57	3.54
χ^2	2.336	2.101	2.178	2.107

Fig. 3a shows the temperature dependence of electrical resistivity for $La_{1.4}Sr_{1.6}Mn_2O_7$. The electrical resistivity increases with increasing temperature, a typical characteristic of metal-like ($d\rho/dT > 0$) temperature dependence, then decreases with increasing temperature, a typical characteristic of nonmetal-like ($d\rho/dT < 0$) temperature dependence. The metal to nonmetal transition occurs in the low temperature region (<120 K). Similar results were also observed in previous reports [7,25]. The temperature dependence of electrical resistivity for $La_{1.4}Sr_{1.6}Mn_2O_7F_2$ is given in Fig. 3b. It can be clearly seen that the electrical resistivity decreases with increasing temperature, a typical characteristic of nonmetal-like ($d\rho/dT < 0$) behavior. The parent compound $La_{1.4}Sr_{1.6}Mn_2O_7$ shows the lowest electrical resistivity among the samples. The electrical resistivity of $La_{1.4}Sr_{1.6}Mn_2O_7$ is 0.51 Ω-cm at 290 K, which is in relatively good agreement with previous reports [7,20,23,25].